Band structure and elastic properties of cavity-type hypersonic phononic crystals fabricated by femtosecond laser-induced two-photon polymerization

A. M. Rakhymzhanov[1,2], A. Gueddida[3,4] , E. Alonso-Redondo[5], Z. N. Utegulov[1,2,a)], D. Perevoznik[6], K. Kurselis[6], B. N. Chichkov[6,7], E. H. El Boudouti[4], B. Djafari-Rouhani[3], G. Fytas[5,8]

[1]*Department of Physics, School of Science and Technology, Nazarbayev University, Astana 010000, Kazakhstan*

[2]*Optics Laboratory, National Laboratory Astana, Nazarbayev University, Astana 010000, Kazakhstan*

[3]*Institut d'Electronique, Microélectronique et Nanotechnologie, Université de Lille 1, Lille, France*

[4]*LPMR, Département de Physique, Faculté des Sciences, Université Mohamed I, 60000 Oujda, Morocco*

[5]*Max Planck Institute of Polymer Research, Ackermannweg 10, 55128 Mainz, Germany*

[6]*Laser Zentrum Hannover e.V., 30419 Hannover, Germany*

[7]*Institute of Laser and Information Technologies RAS, Moscow, Troitsk, Russia*

[8]*Department of Materials Science, University of Crete and FORTH, 71110 Heraklion, Greece*

The phononic band diagram of a periodic square structure fabricated by femtosecond laser pulse-induced two photon polymerization is recorded by Brillouin light scattering (BLS) at hypersonic (GHz) frequencies and computed by finite element method. The theoretical calculations along the two main symmetry directions quantitatively capture the band diagrams of the air-and liquid-filled structure and moreover represent the BLS intensities. The theory helps identify the observed modes, reveals the origin of the observed bandgaps at the Brillouin zone boundaries and unravels direction dependent effective medium behavior.

Phononic crystals (PnC), the acoustic analogues of photonic crystals, are periodic structures made of materials with different acoustic impedances. The main consequence of the structure periodicity is the formation of band gaps in the phonon dispersion at certain wavelengths commensurate with the lattice constant. PnC with periodicity in the sub-micrometer range can block hypersonic phonons with potential applications in compact wireless and sensing devices.[1,2] Control over the GHz phonons in polymers and semiconductors could lead to the design of new highly efficient hybrid photonic–phononic signal processing technologies.[3] Devices in the optoelectronics industry such as resonators, cavities and waveguides can be realized in a phononic crystal by removal or distortion of the inclusions.[1,4]

_____

[a)] Author to whom correspondence should be addressed. Electronic mail: zhutegulov@nu.edu.kz.

Since the first realization of a hypersonic phononic band gap,[5] the design, fabrication and characterization of 1D, 2D and 3D hypersonic phononic crystals (hPnC) has been the subject of intensive research.[6-14] However, the fabrication of such periodic crystals is still a technological challenge, since control over the periodicity for various 3D architectures on the sub micrometer scale is necessary. Electron and focused ion-beam lithographic techniques are powerful in producing 2D GHz phononic structures in opaque media.[15,16] Self-assembly by vertical lifting deposition[5,7] and holographic interference lithography[6,17,18] have enabled fabrication of 2D hPnC in transparent polymeric media with limited 3D architectures. To realize true multiple 3D nano- and micro-structured structures in photosensitive polymeric media, direct laser writing technology based on multi-photon absorption processes such as *two-photon polymerization* (2PP) is a very attractive option.[19-21] Because of the threshold behavior and nonlinear nature of the 2PP process, small spatial features with optical resolution beyond the diffraction limit can be achieved. By scanning the focused laser spot inside a photo-resist various predefined 3D topographic shapes can be formed. So far 2PP technique has been applied for the fabrication of 2D and 3D photonic crystals.[22-27] but we are not aware of its utilization in phononics. In this work, we use femtosecond laser 2PP to fabricate square lattice hPnCs based on zirconium propoxide-based hybrid sol-gel photosensitive material.[26]

There are few reports on cavity-type hPnCs with cylindrical nanopores, e.g. with a single crystalline epoxy/air sample[18] and anodic porous alumina containing hexagonal arrays of aligned nanopores oriented normal to the film surface[27]. Using Brillouin light scattering spectroscopy (BLS), the phonon dispersion relation has been recorded for a square lattice hPnC with filled spherical nanopores[6] and hexagonal lattice with both air-and filled spherical nanopores.[27] In the former case, there was no direct comparison with the theoretical band diagram, while in the latter this comparison was restricted on the observed phononic branches. For a fundamental understanding, however, the theoretical representation of the full BLS spectrum, frequencies and intensities, is necessary. Here, we report on the experimental band diagram of both air and filled square nanopores in a square lattice recorded by BLS and thorough theoretical calculations of the dispersion and the BLS intensities.

The band structure of the square lattice polymer-based hPnC is sensitive to the pore shape as illustrated in Fig. 1 for air-filled holes, lattice parameter $a = 740$nm, filling fraction $f = 0.46$ and elastic properties representing the hPnC of this study. This problem was studied theoretically for *periodic fibre reinforced composite* solid materials[29] and solid square rods in air[30] enabling tunability of the band gap by rotating the rods. The effect of the inclusion shapes or varying geometry in architected materials is of current research interest.[31] The phonon dispersion curves are calculated for a 2D crystal being infinite along the z direction to avoid superposition with the numerous modes propagating in the substrate and represent the in-plane modes polarized in the (x,y) plane. The calculation is performed by using finite element method and the dispersion curves present the frequency as a function of the Bloch wave vector $\mathbf{k} = (k_x, k_y)$ along the high symmetry axes (ΓX and ΓM) of the Brillouin zone (BZ). The band structures for square lattice symmetry clearly depend on whether the inclusions are of circular and rotated-square shapes (Fig. 1b and c). Absolute band gap can be opened in the rotated-square structure and even in the circular geometry, whereas the non-rotated square shape yields partial band gaps (along ΓM).
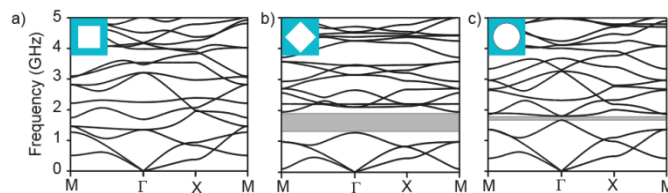

FIG. 1. Dispersion curves of square lattice polymer based phononic crystal with square (a), rotated-square (b) and circular (c) holes. The lattice parameter, filling fraction and density are, respectively, $a = 740$nm, $f = 0.46$ and $\rho = 1190$ kg/m^3, whereas the longitudinal and transverse sound velocity in the matrix assumes $c_L = 2900$ m/s and $c_T = 1700$ m/s (see text).

To realize such periodic structures, we synthesized the photoresist[26] and used it as a platform for its subsequent polymerization with lateral 2D periodicity.The focal spot of the writing pulse laser beam (517 nm, 60 fs, 76 MHz, 70 mW) was accurately scanned (2 mm/s in a vertical and lateral plane of the transparent pre-baked Zr-propoxide (ZPO) photoresist.[32] Fabrication of a 1x1 mm^2 sample required about 8hours.To remove the non-polymerized material, the sample was developed in 1-propanol. Top view scanning electron micrograph of the 2D-hPnC by 2PP is shown in Fig. 2a along with the schematic picture in Fig. 2c yielding a filling fraction, $f = 0.46$. The two main crystallographic directions ΓM (110) and ΓX (100) are indicated by the arrows.

The phonon band structure of the air-filled and infiltrated hPnC was characterized by BLS spectroscopy. It is based on the elasto-optic interaction of the incident light with thermally activated phonons that results in a Brillouin double shift ($\pm \omega$) in the spectrum of homogeneous media; nanostructured media display much richer spectrum.[5,7,12,14] In the present hPnC, phonons were probed with wave vector $\mathbf{q} = \mathbf{k_s} - \mathbf{k_i}$ (Fig. 2d) lying along the ΓX and ΓM (Fig. 1b); $\mathbf{k_i}$ ($\mathbf{k_s}$) is the incident (scattered) light wave vector. The magnitude, $q = 4\pi/\lambda \sin(\theta/2)$, is determined by the angle θ between $\mathbf{k_i}$ and $\mathbf{k_s}$ where $\lambda = 532$ nm is the wavelength of the laser beam. Figure 2b displays the image of the diffracted pattern of the laser beam impinging on hPnC and the red arrows (in Fig. 2a,b) mark the direction (ΓX or ΓM) of the probing wave vector $\mathbf{q}$.
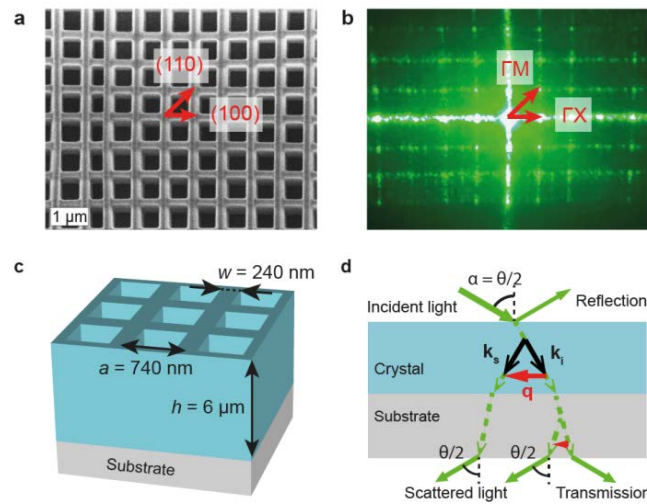

FIG. 2. Scanning electron micrograph (a) (top view) and schematic representation (c) of the structure with the two main crystallographic directions indicated by the red arrows in (a). (b) Photograph of the optical diffracted pattern with the two symmetry directions marked by the red arrows. (d) Lateral view of the Brillouin scattering geometry with $\mathbf{k_i}$, $\mathbf{k_s}$ and q being the wave vectors of the incident and scattered light, and probed phonon, respectively.

For the air-filled hPnC, the dispersion relation was recorded only along ΓM due to very strong elastic (Rayleigh) scattering along ΓX. Experimental BLS spectra at $q < q_{ΓM} \sim 6 \cdot 10^{-3}$ nm^{-1}) represented by Lorentzian lines (red) are shown in Fig. 3a. Since an independent access to the elastic properties of the unstructured material was not feasible, we rely on their determination searching for the optimal theoretical description of the full BLS spectra, i.e., dispersion, polarization and relative peak intensities. As the spectra were recorded with q's extending beyond the first BZ, we show the unfolded dispersion relation into the second BZ in Fig. 3b and Fig. S1. The branches are colored according to their polarization (longitudinal, L, versus transverse, T) character. Based on the band sorting method,

$$P_X = \frac{\iint_{u.cel} |uX|^2 dS}{\iint_{u.cel} (|u_x|^2 + |u_y|^2) dS}$$ (1)

where X is a direction parallel to the wave vector and u_X represents the projection of the displacement field along this direction; [1,1] for ΓM and [1,0] for ΓX. For P_X close to 1(0), the corresponding mode has predominantly longitudinal (transverse) polarization; the value of P_X is highlighted by a color bar in Fig. S1. The dispersion curves are given for two different choices of the acoustic velocities: c_L = 2900 m/s, c_T = 1400 m/s in Fig. S1a and c_L = 2900m/s, c_T = 1700m/s in Fig. S1c. While both choices lead to a good agreement with the experimental phonon dispersion, the higher c_T appears more satisfactory because it captures the longitudinal character of the observed modes. The value of c_L in the range (2700 - 2900) m/s does not influence the agreement between the theoretical and experimental dispersion curves.
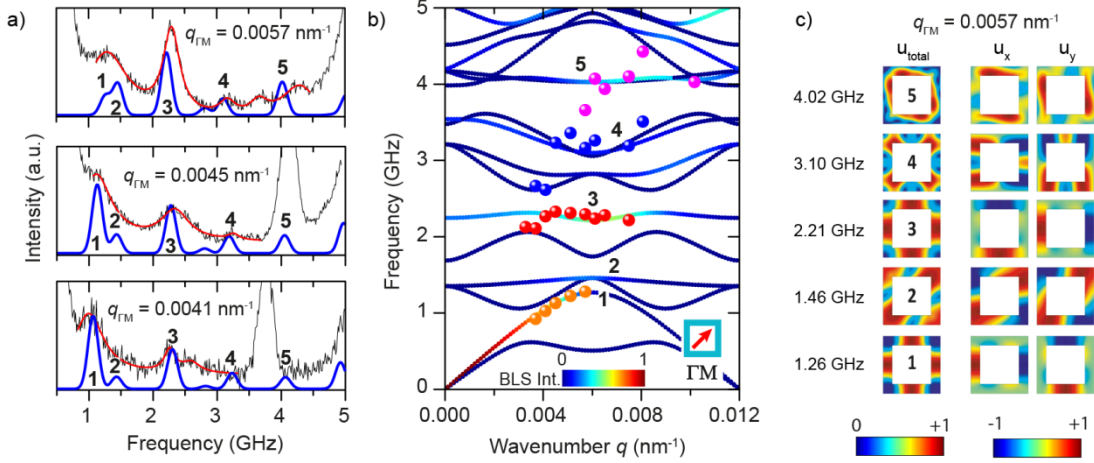

FIG. 3. a) Experimental (black) and theoretical (blue) BLS spectra of the hPnC with air-filled square nanopores at three wave vector q's along the ΓM direction. The very strong peaks in the experimental spectra at the two lowest q's (around 3.8 and 4.1 GHz) belong to the longitudinal phonon in the glass substrate. The experimental spectra were represented by Lorentzian shapes (red lines). (b) Theoretical (lines) and experimental (dots) band diagrams along ΓM direction. The color scale denotes the strength of the BLS intensity. (c). Displacement fields for the modes at the wave number $q_{ΓM}$ = 0.0057 nm^{-1} with increasing frequency. The color bars indicate the amplitude of the displacement.

The uniqueness of the velocity values can be verified by a more stringent criterion which is the prediction of the BLS intensity.[12,32] Based on the photoelastic mechanism of the light-matter interaction (Eq. S1), the polarized (VV) BLS intensity for acoustic waves propagating along the ΓM direction (see Eq. S1),

$$I = |E^s|^2 \propto \left| \frac{1}{\omega} \iint_{unit.cell} e^{i\vec{q}\vec{r}} \left[(P_{11} + P_{12}) \times \left(\frac{\partial u_x}{\partial x} + \frac{\partial u_y}{\partial y} \right) - 2 \times P_{66} \times \left(\frac{\partial u_x}{\partial y} + \frac{\partial u_y}{\partial x} \right) \right] E^I dS \right|^2$$ (2)

depends on the photoelastic coefficients $P_{11}+P_{12}$ and P_{66} ; for isotropic materials, $P_{66} = (P_{11}-P_{12})/2$. To compare with the relative intensities in the BLS spectra, there is only the ratio $P_{66}/(P_{11}+P_{12})$ which is used as a free parameter. The best qualitative agreement was found when $P_{66}/(P_{11}+P_{12})$ is negative and relatively small (about -0.2, $P_{11}/(P_{11}+P_{12})$ = 0.3 and $P_{12}/(P_{11}+P_{12})$ = 0.7, Fig. S1 b,d). Since there is no additional source of information, a negative P_{66}, i.e., a destructive addition in Eq.2 is needed for an adequate theoretical representation of the BLS intensities.

The assignment of the observed branches and the appearance of the band gap (between modes **1** and **3**) in Fig.3 can be ambiguous in the absence of rigorous theoretical calculations of the full BLS experiment. In fact, the experimental band gap concerns only branches with a high longitudinal character, whereas the theory predicts a smaller unidirectional stopband (Fig. 1 and 3). To provide more insight into the nature of the observed branches,

maps of the displacement fields for the modes close to the first BZ boundary are displayed in Fig. 3c with increasing frequency at $q_{\Gamma M} = 0.0057$ nm^{-1}. Note that mode **2** is strongly longitudinal (vibration along the ΓM direction), whereas both modes **1** and **3** possess mixed polarization (Fig. S1d). Their motion corresponds to successive contraction/dilatation of both sides of the square, while the corners are kept almost fixed. In the evaluation of the BLS intensity (Eq. 2), the main contribution to the strain arises from the second term for mode **1** and the first term for modes **2** and **3**.

The strong diffraction and the occurrence of the BZ along ΓX at lower q (= 0.004nm^{-1}) than for ΓM (Fig.1) renders the experimental access along ΓX ambiguous. To reduce the strong elastic scattering, we proceed with filled nanopores[5,6] infiltrating the hPnC with Cargille (**F**) liquid (refractive index, $n_F = 1.513$) almost optically matching the ZPO matrix ($n_Z = 1.51$). Although the infiltration reduces the impedance contrast, the mismatch between corresponding sound velocities and densities of ZPO and **F** liquid is sufficient to allow an acoustic Bragg interference. Such band gap along two symmetry directions is displayed in the phonon dispersion of Fig. 4a,d.

The theoretical dispersion curves for the filled-hPnC are considered in Fig. 4 along ΓX and ΓM and are again unfolded into the second BZ; the coloring is according to the longitudinal versus transverse character (Fig. S2). In the calculations, the longitudinal sound velocity in **F** is fixed to its bulk value ($c_f = 1670$m/s), while the acoustic velocities in the solid ZPO are fixed to $c_L = 2900$ m/s and $c_T = 1400$m/s (Fig. S2a-d) or $c_T = 1700$ m/s (Fig. S2e-h), as in the case of the air-filled hPnC (Fig. S1). To investigate which longitudinal modes contribute significantly to the BLS spectra, the computation of their intensities includes now the photoelastic coefficient, P, in **F** liquid as adjustable parameter (Eq. S2).Good agreement with the experimental spectra was expectedly obtained with a higher P in the fluid compared to (P$_{11}$+P$_{12}$) in the ZPO solid; P/(P$_{11}$+P$_{12}$) = 4 (Fig. S3). While both c_T values lead to a good agreement between theory and experiment along ΓX, the branches in the band diagram along ΓM are not represented equally well with either c_T value; lowest (highest) branches favor the lower (higher) c_T value (Fig. S2b,d). We note that the air-filled (Fig. 3) and infiltrated (Fig.4) films used in this study are not the same and their fabrication can tolerate somewhat different c_T values. Hence, a closer estimate of this quantity is not justified without additional physical arguments. Nevertheless, the full representation of the BLS experiment is the correct approach to yield the elastic and photoelastic parameters of the hPnC constituent components at nanoscale. We have also examined an alternative approach assuming a solidification of **F** next to the wall[28]. A thin (~10nm) solidified layer at the interface with low transverse acoustic velocity (~100 m/s) creates few additional features (flat branches) in the band diagram but are not identifiable among the experimental branches.
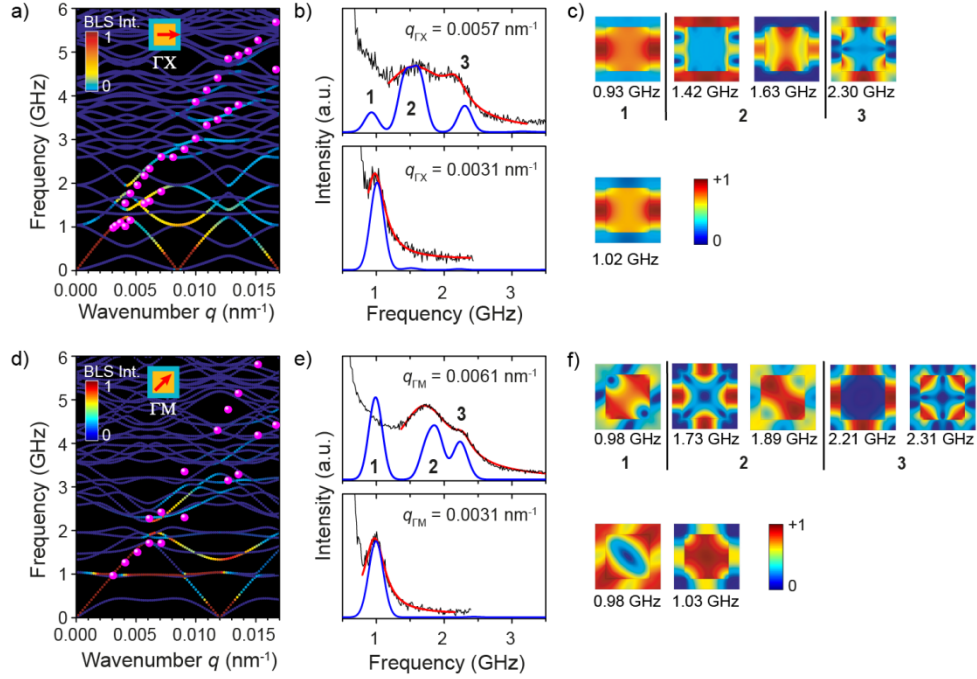
FIG. 4. The experimental (pink circles) and theoretical (lines) band diagrams (a,d), the experimental (black) and theoretical (blue) BLS spectra at two wave vector q's (b,e), and the displacement fields for the observed modes (c,f) of the filled hPnC along the ΓX (a-c) and ΓM (d-f) directions. The experimental spectra were represented by a sum of Lorentzian shapes (red lines in b,e).

The effective sound velocity, c_{eff}, at long wavelengths, obtained from the dispersion relations at sufficiently low q's (Fig. 4a,d), is distinct along the two symmetry directions. Indeed, the theory (Fig. 5) predicts about 13% higher value ($c_{\text{eff}} = 2320$ m/s) along ΓX than along ΓM ($c_{\text{eff}} = 2040$ m/s).The effective sound velocity in the air-filled hPnC displays the same trend and the reduction compared to the filled counterpart is direction dependent; from about ~15% along ΓM to ~5% along ΓX (Fig. 5). The observed anisotropy of the effective sound velocity is expected in view of the symmetry of the square lattice, in contrast to an isotropic behavior in a triangular lattice hPnC with circular nanopores. Triggered by this unpredicted observation, we computed c_{eff} as a function of the filling fraction also for two filling liquids with different fluid velocity, c_f (1670 m/s and 1000 m/s in Fig.S4). There is no linear dependence of c_{eff} to c_f and certainly the common Wood's law fails.
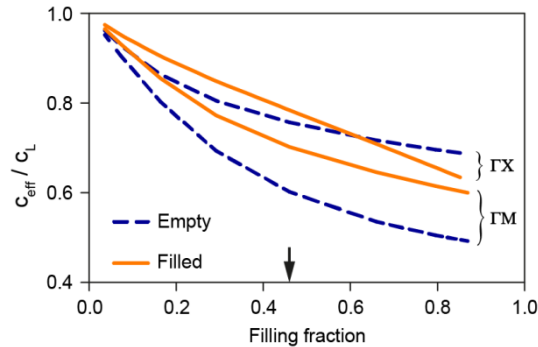

FIG. 5. Effective sound velocity (c_{eff}) normalized to the longitudinal sound velocity of the matrix (c_L) along ΓX and ΓM. The arrow indicates the filling fraction of the present hPnC.

The displacement fields associated to the modes that contribute to BLS are presented in Fig. 4c,f for some selected values of the wave vector. For instance, along ΓX, the mode at the frequency 1.02 GHz and $q = 0.0031$ nm^{-1} is longitudinal and its contribution to BLS mainly arises from the fluid hPnC component. For $q = 0.0057$ nm$^-$

[1], the modes at 1.42 GHz and 1.63 GHz are mainly longitudinal whereas the mode at 2.30 GHz is of mixed character. We note that the peak termed **2** results from the contributions of two modes at 1.42 GHz and 1.63 GHz. Similarly, in the case of ΓM direction, some of the peaks result from the contribution of two close modes (Fig. 4e). Overall, filling of the holes strongly impacts hPnC the band structure as well as the nature of the probed modes by BLS. It includes the change in c_{eff}, the penetration of the displacement field into the fluid and the activation of high frequency modes along the c_{eff}-line.

Summing up, the present experimental and theoretical study demonstrates the effect of the shape of the holes on the direction-dependent hypersonic phononic properties (Fig. 1) of a cavity with square lattice symmetry fabricated by femtosecond laser pulse-induced two photon polymerization technique. Filling the holes with a fluid strongly modifies the phononic band diagram being a necessary condition for sensor applications.[34] Yet, we have theoretically examined the tuning sensitivity to the filling material, fraction and shape of the inclusions in square lattice phononics that calls for experimental verification. The full representation of the experiment (band structure and intensities) is necessary to yield a unique identification of all probed vibration modes and the effective medium sound velocity. A detailed understanding of phonon propagation in periodic structures is a precondition to access fundamental concepts of strong phonon-photon interactions and thermal properties.[35,36]

1. R. H. Olsson,et. al, International Ultrasonics Symposium Rome, Italy, 20-23 September 2009, IEEE, 1150 (2009).
2. S. Mohammadi, A. A. Eftekhar, A. Khelif, W. D. Hunt and A. Adibi. Appl. Phys. Lett. 92, 221905 (2008).
3. J.-H. Lee, C. Y. Koh, J. P. Singer, S.J. Jeon, M. Maldovan, O. Stein and E. L. Thomas. Adv. Mater. **26**, 532 (2014).
4. M. Ziaei-Moayyed, et al., 24th International Conference on Micro Electro Mechanical Systems , Cancun, Mexico, 23 - 27 January 2011, IEEE, pp. 1377 (2011).
5. W. Cheng, J. Wang, U. Jonas, G. Fytas, and N. Stefanou, Nat. Mater. **5**, 830 (2006).
6. T. Gorishnyy, J. Jang, C.Y. Koh, and E. L. Thomas, Appl. Phys. Lett. **91**, 121915 (2007).
7. T. Still, W. Cheng, M. Retsch, R. Sainidou, J. Wang, U. Jonas, N. Stefanou and G. Fytas. Phys. Rev. Lett. **100**, 194301 (2008).
8. A. V. Akimov, Y. Tnaka, A. B. Pevtsov, S. F. Kaplan, V. G. Golubev, S. Tamura, D. R. Yakovlev, and M. Bayer. Phys. Rev. Lett. **101**, 033902 (2008).
9. P. M. Walker, J. S. Sharp, A. V. Akimov, and A.J. Kent, Appl. Phys. Lett. **97**, 073106 (2010).
10. V. L. Zhang, F. S. Ma, H. H. Pan, C. S. Lin, H. S. Lim, S. C. Ng, M. H. Kouk, S. Jain, and A. O adeyeye. Appl. Phys. Lett. **100**, 163118 (2012).
11. G. Zhu, N. Z. Swinteck, S. Wu, J. S. Zhang, H. Pan, J. D. Bass, P. A. Deymier, D. Banerjee, and K. Yano. Phys. Rev. B **88**, 144307 (2013).
12. D. Schneider, F. Liaqat, E. H. El Boudouti, O. El Abouti, W. Tremel, H.-J. Butt, B. Djafari-Rouhani, and G. Fytas. Phys. Rev. Lett. **111**, 164301 (2013).
13. S Wu, G. Zhu, J. S. Zhang, D. Banerjee, J. D. Bass, C. Ling, and K. Yano. Phys. Chem. Chem. Phys. **16**, 8921 (2014).
14. P. Beltramo, D. Schneider, G. Fytas, and E. M. Furst. Phys. Rev. Lett. **113**, 205503 (2014).

15. D. F. Goettler, M. F. Su, C. M. Reinke, S. Alaie, P. E. Hopkins, R. H. Olsson III, I. El-Kady, and Z. C. Leseman. AIP Adv. **1**, 042001 (2011).
16. V. L. Zhang, C. G. Hou, H. H. Pan, F. S. Ma, M. H. Kuok, H. S. Lim, S. C. Ng, M. G. Cottam, M. Jamali, and H. Yang. Appl. Phys. Lett. **101**, 053102 (2012).
17. J. Li, and S. Yang, Microelectron. Eng. **128**, 7 (2014).
18. T. Gorishnyy, C. K. Ullal, M. Maldovan, G. Fytas, and E. L. Thomas. Phys. Rev. Lett. **94**, 115501 (2005).
19. S. Maruo, O. Nakamura, and S. Kawata, Opt. Lett. **22**, 132 (1997).
20. J. Serbin, A. Egbert, A. Ostendorf, B. Chichkov, R. Houbertz, G. Domann, J. Schulz, C. Cronauer, L. Fröhlich, and M. Popall. Opt. Lett. **28**, 301 (2003).
21. L. Montemayor, V. Chernow and J. R. Greer. MRS Bull. **40**, 1122 (2015).
22. H. B. Sun, S. Matsuo and H. Misawa. Appl. Phys. Lett. **74**, 786 (1999).
23. J. Serbin, A. Ovsianikov, and B. N. Chichkov, Opt. Express **12**, 5221 (2004).
24. M. Deubel, G. von Freymann, M. Wegener, S. Pereira, and K. Busch. Nat. Mater. **3**, 444 (2004).
25. R. Guo, Zh. Li, Z. Jiang, D. Yuan, W. Huang, and A. Xia. J. Opt. A: Pure Appl. Opt. **7**, 396 (2005).
26. A. Ovsianikov, J. Viertl, B. Chichkov, M. Oubaha, B. MacCraith, I. Sakellari, A. Giakoumaki, D. Gray, M. Vamvakaki, M. Farsari, and C. Fotakis. ACS Nano **2**, 2257 (2008).
27. M.V. Rybin, I.I. Shishkin, K.B. Samusev, P. A. Belov, Y.S. Kivshar, R. V. Kiyan, B. Chichkov, and M.F. Limonov. Crystals **5**, 61 (2015).
28. A. Sato, Y.Pennec, T. Yanagishita, H. Masuda, W. Knollm, B. Djafari-Rouhani, and G. Fytas. New J. Phys. **14**, 113032 (2012).
29. J. Vasseur, B. Djafari-Rouhani, L. Dobrzynski, M. S. Kushwaha, and P. Halevi. J. Phys.: Condens. Matter **7**, 8759 (1994).
30. C. Goffaux and J. P. Vigneron. Phys. Rev. B **64**, 075118 (2001).
31. S. Babaee, N. Viard, P. Wang, X. Fang, and K. Bertoldi. Adv. Mater. DOI:10.1002/adma.201504469 (2015).
32. M. Farsari, B. N. Chichkov, Nat. Photonics **3**, 450 (2009).
33. D. Schneider, F. Liaqat, El H. El Boudouti, Y. El Hassouani, B. Djafari-Rouhani , W. Tremel, H.-J. Butt, and G. Fytas. Nano Lett., **12**, 3101 (2012).
34. S. Amoudache, Y. Penner, B. Djafari-Rouhani, A. Khater, R. Lucklum, and R. Tigrine. J. Appl. Phys **115**, 134503 (2014).
35. M. M. Maldovan. Nature **503**, 209 (2013).
36. S.Volz J. Ordonez-Miranda, A. Shchepetov, M. Prunnila, J. Ahopelto, T. Pezeril, G. Vaudel, V. Gusev, P. Ruello, E. M. Weig, M. Schubert, M. Hettich, M. Grossman, T. Dekorsy, F. Alzina, B. Graczykowski, E. Chavez-Angel, J. S. Reparaz, M. R. Wagner, C. M. Sotomayor-Torres, S. Xiong, S. Neogi and D. Donadio' Eur. Phys. J. B **15**, 89 (2016).